2025 IEEE 36th Annual International Symposium on Personal, Indoor and Mobile Radio Communications (PIMRC): Track 4: Emerging Technologies, Applications and Platforms

2025 IEEE 36th International Symposium on Personal, Indoor and Mobile Radio Communications (PIMRC) | 979-8-3503-6323-4/25/$31.00 ©2025 IEEE | DOI: 10.1109/PIMRC62392.2025.11275258

# Channel Estimation via Digital Twins with Limited a Priori Knowledge

Lorenzo Del Moro[1], Francesco Linsalata[1], Marouan Mizmizi[1],
Damiano Badini[2], Umberto Spagnolini[1] and Maurizio Magarini[1]
[1]*Dipartimento di Elettronica, Informazione e Bioingegneria, Politecnico di Milano, Milan, Italy*
[2]*Huawei Technologies Italia S.r.l., Segrate*
Email: [1]{name.surname}@polimi.it, [2]damiano.badini@huawei.com

***Abstract*—Digital Twin (DT) has emerged as a promising solution for channel estimation. By leveraging high-resolution 3D models of the scenario and ray-tracing simulations, DT could provide valuable site-specific prior knowledge on the channel's space-time (ST) invariant features of the multipath environment, such as angles of arrival, angles of departure, and propagation delays. However, the real-time characterization of these features imposes computational constraints on ray-tracing simulations, hence limiting the prior knowledge of the multipath environment and corresponding ST features, and degrading estimation accuracy. In this paper, we propose and investigate, for the first time, three distinct DT-empowered low-rank methods for channel estimation, under different degrees of prior knowledge corresponding to limited number of paths provided by DT. Specifically, these methods perform modal projection onto a joint space-time, a spatial, and a temporal subspace. We compare our proposed methods with state-of-the-art techniques, and evaluate their performance in a synthetic scenario. Numerical results show that robustness, when prior knowledge is limited to few paths, is achieved when exploiting only temporal features, while estimation accuracy is attained when joint space-time features are considered.**

***Index Terms*—Channel estimation, Low Rank, Digital Twin**

## I. Introduction

Accurate channel estimation is a critical challenge to achieve high-performance in wireless communication systems that exploit precoding/combining schemes. However, recent research trends are pushing towards increasing the number of transmitting and receiving antennas $(N_{\mathrm{T}}, N_{\mathrm{R}})$, and bandwidth $B$ [1], [2]. Hence, as channel estimation accuracy degrades with the dimensionality of the resulting multiple-input multiple-output (MIMO) channel, the need for efficient channel estimation is mandatory for next-generation wireless networks. A promising solution for channel estimation, is the concept of Digital Twin (DT) [3], [4]. By leveraging high-resolution 3D models and opportunistic ray-tracing simulations, DT-supported wireless networks can generate accurate and dynamic digital representations of the electromagnetic environment [5], [6], thus providing valuable prior knowledge.

The work was partially supported by the European Union under the Italian National Recovery and Resilience Plan (NRRP) of NextGenerationEU, partnership on "Telecommunications of the Future" (PE00000001 - program "RESTART", Structural Project 6GWINET). This work is within the Joint Lab between Politecnico di Milano and Huawei.

DT-empowered channel estimation methods, leverage the prior information on the space-time (ST) invariant features, such as angles of arrival (AoAs), angles of departure (AoDs), and delays, associated to the multipath propagation environment [7], [8]. The prior information made available from DT can be used to characterize the propagation modes of the MIMO channel, which are intrinsically related to the large-scale geometry of the environment [9]. It follows that, these methods are robust to small-scale geometric inconsistencies and material mismatches between the 3D model and the real-world environment. This eliminates the need for precise geometric and electromagnetic data or calibration procedures, which are typically required for accurate phase information in ray-tracing simulations [10]. Furthermore, the slowly time-varying channel's ST features are easily tracked in comparison to the fast time-varying components, i.e. fading amplitudes, which are influenced by small-scale effects. What above allows the DT to maintain accurate and updated information on the channel's ST features.

Unfortunately, despite the high estimation accuracy achieved with DT-empowered channel estimation methods, a main concern remains in the restricted number of paths that the DT can extract. In fact, due to computational constraints for real-time characterization of the propagation environment, the DT only provides limited prior information on the multipath components, through time-constrained ray-tracing simulations. As a result, a trade-off between accurate prior information and real-time characterization is a mandatory aspect in DT-empowered channel estimation.

In [7], we proposed a DT-empowered low-rank (LR) channel estimation approach, which performs modal projection on separate space and time (SST) subspaces. However, despite we defined a DT framework and presented theoretical and simulation results, a performance analysis, under different levels of prior information, in terms of paths provided by DT, is missing. To this aim, in this paper, we propose and investigate for the first time three distinct DT-empowered LR channel estimation approaches under limited a priori information; a DT joint space-time (DT-JST) LR method, a DT spatial (DT-S) LR method, and a DT temporal (DT-T) LR method. Specifically, the proposed approaches perform modal projection on a joint space-time, a spatial, and a temporal subspace, respectively.

**Contributions** The key contributions of this work are summarized as follows.

- Propose and provide a theoretical analysis of DT-JST, a DT-S, and DT-T approach for channel estimation, which exploit, in different manner, prior knowledge on ST invariant channel's features derived from the DT.
- Compare our proposed approaches with the DT-SST method [7] and the conventional LS, in terms of normalized mean squared error (NMSE), when limited multipath components are provided by DT.
- Show that, in terms of NMSE, the DT-T method is suitable when few paths are provided, while the DT-JST exhibits greater performance, when accurate prior information is available. Specifically, under a constraint of $\tilde{P}$ paths, the DT-JST gains over 20 dB against the state of the art LS approach, whereas for $\tilde{P} = 1$ path, the DT-T overperforms the LS of at least 5 dB, for Signal-to-Noise Ratio (SNR) values ranging from $-30$ dB to 15 dB.

**Organization** The rest of the paper is organized as follows. Section II introduces the system model, while Section III proposes our distinct DT-empowered LR channel estimation methods. In Section IV numerical results are presented. Section V concludes the work and suggests future exploration.

**Notation** $(\cdot)^*$, $(\cdot)^{\mathsf{T}}$ and $(\cdot)^{\mathsf{H}}$ denote the complex conjugate, matrix transpose, Hermitian transpose. The Kronecker product is $\otimes$, $\mathrm{diag}(\mathbf{v})$ is a diagonal matrix with vector $\mathbf{v}$ on main diagonal, and $\mathrm{vec}\{\mathbf{A}\}$ is the stacking operator, such that $\mathrm{vec}\{\mathbf{ABC}\} = (\mathbf{C}^T \otimes \mathbf{A})\mathrm{vec}\{\mathbf{B}\}$ and $\mathrm{vec}\{\mathbf{AB}\} = (\mathbf{I} \otimes \mathbf{A})\mathrm{vec}\{\mathbf{B}\}$. Additionally, $\mathrm{Tr}\{\mathbf{A}\}$ is the trace of the square matrix $\mathbf{A}$, $\mathbb{E}\{\cdot\}$ denotes the expectation, and $\mathbf{I}_N$ is the $N \times N$ identity matrix.

## II. System Model

We consider a MIMO orthogonal frequency-division multiplexing (OFDM) system with a base station (BS) and a user equipment (UE) equipped with $N_{\mathrm{R}}$ and $N_{\mathrm{T}}$ antenna elements, respectively. The duration of an OFDM symbol is given by $T = (N_{\mathrm{sc}} + N_{\mathrm{cp}})T_{\mathrm{s}}$, where $T_{\mathrm{s}} = \frac{1}{B}$ represents the sampling interval for a system bandwidth $B$, $N_{\mathrm{cp}}$ is the length of the cyclic prefix (CP), and $N_{\mathrm{sc}}$ denotes the number of subcarriers.

### A. Uplink Pilot Transmission

In pilot-based OFDM systems, channel estimation is achieved through the transmission of $N_{\mathrm{p}}$ symbols from each antenna, which are known both at the transmitter and receiver. These known symbols are scattered on a time-frequency grid, corresponding to predetermined subcarriers and specific training OFDM symbols [9]. Here, we assume that each OFDM training symbol experiences a fading realization. Differently, the channel's ST features, which depend on the large-scale geometry of the environment, are assumed to be static in $M$ OFDM training symbols [11].

Let $\mathbf{X}_m^{(n_{\mathrm{T}})} \in \mathbb{C}^{N_{\mathrm{p}} \times 1}$ be the vector containing the baseband transmitted complex samples allocated for piloting at $n_{\mathrm{T}}$th antenna, with $n_{\mathrm{T}} = 1, \ldots, N_{\mathrm{T}}$, and in the $m$th OFDM training symbols, with $m = 1, \ldots, M$. We call $\eta$ the transmitted power per subcarrier and per antenna. Assuming a sufficiently long CP to prevent inter-symbol interference, the vector of complex baseband received pilot samples, in the $m$th OFDM training symbol, and antenna $n_{\mathrm{R}} = 1, \ldots, N_{\mathrm{R}}$, is expressed as [11]

$$\mathbf{Y}_m^{(n_{\mathrm{R}})} = \sum_{n_{\mathrm{T}}=1}^{N_{\mathrm{T}}} \mathrm{diag}\big(\mathbf{X}_m^{(n_{\mathrm{T}})}\big)\mathbf{H}_m^{(n_{\mathrm{R}},n_{\mathrm{T}})} + \mathbf{w}_m^{(n_{\mathrm{R}})}, \tag{1}$$

where $\mathbf{w}_m^{(n_{\mathrm{R}})} \in \mathbb{C}^{N_{\mathrm{p}} \times 1}$ denotes the vector of additive white Gaussian noise (AWGN), with i.i.d. elements of variance $\sigma_w^2$, and $\mathbf{H}_m^{(n_{\mathrm{R}},n_{\mathrm{T}})} \in \mathbb{C}^{N_{\mathrm{p}} \times 1}$ is the frequency-domain channel across the $N_{\mathrm{p}}$ subcarriers. This is obtained through the Discrete Fourier Transform (DFT) of the channel impulse response as

$$\mathbf{H}_m^{(n_{\mathrm{R}},n_{\mathrm{T}})} = \bar{\mathbf{F}}\mathbf{h}_m^{(n_{\mathrm{R}},n_{\mathrm{T}})}, \tag{2}$$

where $\mathbf{h}_m^{(n_{\mathrm{R}},n_{\mathrm{T}})} = \big[h_m^{(n_{\mathrm{R}},n_{\mathrm{T}})}(0), \ldots, h_m^{(n_{\mathrm{R}},n_{\mathrm{T}})}(W-1)\big]^{\mathsf{T}}$ is the channel impulse response, within the temporal support length $W$, and $\bar{\mathbf{F}} \in \mathbb{C}^{N_{\mathrm{p}} \times W}$ is the DFT matrix, with entries $[\bar{\mathbf{F}}]_{k,w} = \frac{1}{\sqrt{N_{\mathrm{sc}}}} \exp\left(-j2\pi f_k w / N_{\mathrm{sc}}\right)$, with $f_k$ denoting the frequency index of pilot subcarrier $k = 0, \ldots, N_{\mathrm{p}} - 1$, and $w = 0, \ldots, W-1$. For notational simplicity, we rewrite (1) as

$$\mathbf{Y}_m^{(n_{\mathrm{R}})} = \mathbf{B}_m \mathbf{h}_m^{(n_{\mathrm{R}})} + \mathbf{w}_m^{(n_{\mathrm{R}})}, \tag{3}$$

where $\mathbf{B}_m = \big[\mathrm{diag}\big(\mathbf{X}_m^{(1)}\big)\bar{\mathbf{F}}, \ldots, \mathrm{diag}\big(\mathbf{X}_m^{(N_{\mathrm{T}})}\big)\bar{\mathbf{F}}\big] \in \mathbb{C}^{N_{\mathrm{p}} \times WN_{\mathrm{T}}}$, and $\mathbf{h}_m^{(n_{\mathrm{R}})} \in \mathbb{C}^{WN_{\mathrm{T}} \times 1}$ is the stacking of the concatenation of $N_{\mathrm{T}}$ channel impulse responses $\mathbf{h}_m^{(n_{\mathrm{R}})} = \big[\mathbf{h}_m^{(n_{\mathrm{R}},1)^{\mathsf{T}}}, \ldots, \mathbf{h}_m^{(n_{\mathrm{R}},N_{\mathrm{T}})^{\mathsf{T}}}\big]^{\mathsf{T}}$. Note that, to avoid aliasing in channel estimation, it is required that $N_{\mathrm{p}} \geq WN_{\mathrm{T}}$. Additionally, optimal pilot design results in equipowered, equispaced, and phase shift orthogonal pilot samples [12].

### B. Channel Model

The channel is characterized by multipath propagation with $P$ distinct paths. For the $p$th path, we call the azimuth and elevation AoA as $\boldsymbol{\theta}_p = \big[\phi_p^{\mathrm{rx}}, \varphi_p^{\mathrm{rx}}\big]$, and the azimuth and elevation AoD as $\boldsymbol{\gamma}_p = \big[\phi_p^{\mathrm{tx}}, \varphi_p^{\mathrm{tx}}\big]$. Similarly, let $\tau_p$ represent the delay associated with the $p$th path. We call $\mathbf{a}_{\mathrm{R}}(\boldsymbol{\theta}_p)$ and $\mathbf{a}_{\mathrm{T}}(\boldsymbol{\gamma}_p)$ the array response vectors at the receiver and transmitter, respectively [13]. Let $\mathbf{A}(\boldsymbol{\theta}_p, \boldsymbol{\gamma}_p) \in \mathbb{C}^{N_{\mathrm{R}} \times N_{\mathrm{T}}}$ be the matrix given by

$$\mathbf{A}(\boldsymbol{\theta}_p, \boldsymbol{\gamma}_p) = \mathbf{a}_{\mathrm{R}}(\boldsymbol{\theta}_p)\mathbf{a}_{\mathrm{T}}(\boldsymbol{\gamma}_p)^{\mathsf{T}}. \tag{4}$$

We model the $w$th tap of the MIMO channel $\bar{\boldsymbol{h}}_m(w) \in \mathbb{C}^{N_{\mathrm{R}} \times N_{\mathrm{T}}}$ as [9], [11]

$$\bar{\boldsymbol{h}}_m(w) = \sum_{p=1}^{P} c_{p,m}\mathbf{A}(\boldsymbol{\theta}_p, \boldsymbol{\gamma}_p)g\big(wT_{\mathrm{s}} - \tau_p\big), \tag{5}$$

where $c_{p,m}$ represents the fading amplitude for the $p$th path and $g(\cdot)$ denotes the pulse shaping response given by the cascade of transmit and receive filters. Let $\bar{\boldsymbol{h}}_m \in \mathbb{C}^{N_{\mathrm{R}}N_{\mathrm{T}} \times W}$ be the concatenation of $W$ taps of the stacking operation on (5). It follows that

$$\bar{\boldsymbol{h}}_m = \mathbf{S}(\boldsymbol{\theta}, \boldsymbol{\gamma})\mathbf{C}_m\mathbf{G}(\boldsymbol{\tau})^{\mathsf{T}}, \tag{6}$$

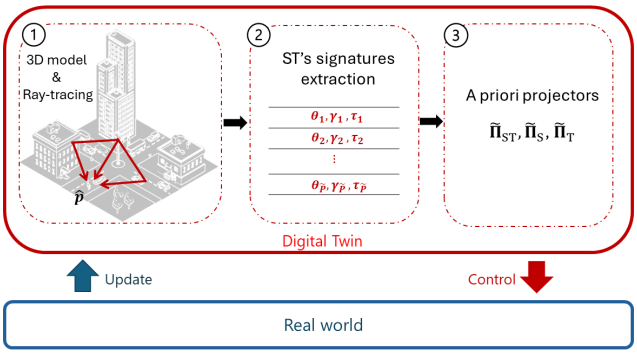


Fig. 1: DT features extraction framework.

where $\mathbf{S}(\boldsymbol{\theta},\boldsymbol{\gamma}) \in \mathbb{C}^{N_\mathrm{R}N_\mathrm{T}\times P}$ is the composition of $P$ vectorized array response matrices, written as

$$\begin{aligned}\mathbf{S}(\boldsymbol{\theta},\boldsymbol{\gamma}) &= \big[\mathrm{vec}\big\{\mathbf{A}(\boldsymbol{\theta}_1,\boldsymbol{\gamma}_1)\big\},\ldots,\mathrm{vec}\big\{\mathbf{A}(\boldsymbol{\theta}_P,\boldsymbol{\gamma}_P)\big\}\big] \\ &= \big[\mathbf{a}(\boldsymbol{\theta}_1,\boldsymbol{\gamma}_1),\ldots,\mathbf{a}(\boldsymbol{\theta}_P,\boldsymbol{\gamma}_P)\big].\end{aligned} \tag{7}$$

Differently, $\mathbf{G}(\boldsymbol{\tau}) = \big[\mathbf{g}(\boldsymbol{\tau}_1),\ldots,\mathbf{g}(\boldsymbol{\tau}_P)\big] \in \mathbb{C}^{W\times P}$ denotes the composition of the $P$ impulse responses, in the temporal support length of the channel, with $\mathbf{g}(\boldsymbol{\tau}_p) = \big[g(-\tau_p),\ldots,g((W-1)T_\mathrm{s}-\tau_p)\big]^\mathsf{T}$, while $\mathbf{C}_m = \mathrm{diag}\big\{[c_{1,m},\ldots,c_{P,m}]\big\} \in \mathbb{C}^{P\times P}$ embodies the fading amplitudes. Moreover, the fading amplitudes are assumed to follow a wide sense stationary uncorrelated scattering (WSSUS) model [11], such that

$$\mathbb{E}\big\{\mathbf{C}_m\mathbf{C}_{m+l}^\mathsf{H}\big\} = \mathrm{diag}\big\{[\alpha_1^2,\ldots,\alpha_P^2]\big\} = \boldsymbol{\Gamma}, \tag{8}$$

with $\alpha_p^2$ being the average instantaneous power for the $p$th path. Finally, the ST MIMO channel vector $\boldsymbol{h}_m \in \mathbb{C}^{N_\mathrm{R}N_\mathrm{T}W\times 1}$ is obtained as stacking of (6). Accordingly, it results in

$$\boldsymbol{h}_m = \sum_{p=1}^{P}\Big(\mathbf{g}(\tau_p)\otimes\mathbf{a}(\boldsymbol{\theta}_p,\boldsymbol{\gamma}_p)\Big)c_{p,m} = \mathbf{T}(\boldsymbol{\theta},\boldsymbol{\gamma},\boldsymbol{\tau})\mathbf{c}_m, \tag{9}$$

where matrix $\mathbf{T}(\boldsymbol{\theta},\boldsymbol{\gamma},\boldsymbol{\tau}) = [\mathbf{t}_1,\ldots,\mathbf{t}_P] \in \mathbb{C}^{N_\mathrm{R}N_\mathrm{T}W\times P}$, with $\mathbf{t}_p = \mathbf{g}(\tau_p)\otimes\mathbf{a}(\boldsymbol{\theta}_p,\boldsymbol{\gamma}_p)$, while $\mathbf{c}_m = \big[c_{1,m},\ldots,c_{P,m}\big]^\mathsf{T} \in \mathbb{C}^{P\times 1}$ is the vector containing the fading amplitudes.

## III. DT-empowered LR methods

Low-rank channel estimation methods have been investigated in the context of multi-slot channel estimation [9], [11], [14]. Specifically, LR approaches estimate MIMO channels by exploiting the invariance of ST features, such as AoAs, AoDs, and delays, across different MIMO channel realizations. These approaches employ modal projection on the received signal to improve estimation accuracy, leveraging the algebraic structure of the MIMO channel and its inherent sparsity. Similarly, in DT-empowered channel estimation, modal projection is employed to improve estimation accuracy [7]. However, the invariance property of the channel's ST signatures is leveraged to enable the DT to generate these features as a priori, in nearly real-time. Specifically, based on the updated UE location $\hat{\mathbf{p}}$ and 3D model of the environment, ray-tracing simulation generates AoAs, AoDs, and delays associated to multipath propagation, as shown in Figure 1. As a result, projectors can be computed as a priori and provided to the physical system for modal projection. This overcomes the latency burden of common LR approaches, which in contrast, require different MIMO realizations to estimate the projectors. Nevertheless, since ray-tracing simulation has complexity $O(\kappa\tilde{P}^n)$, where $\kappa$ is a parameter depending on the scenario and $n$ depends on the ray-tracing technology used, typically ranging between 1 and 2, AoAs, AoDs, and delays are restricted to only $\tilde{P}$ paths, where $\tilde{P} < P$ [5]. In particular, the limited number of paths provides only partial knowledge on the propagation modes of the MIMO channel. As a result, modal projection is performed onto a restricted subspace, which improves estimation accuracy in the low SNR region, due to noise projection. However, this approach can severely degrade estimation accuracy in the high SNR region. Accordingly, in the following, we present three distinct approaches, suited to different levels of prior information, in terms of known multipath components of the propagation environment.

### A. DT-JST method

The DT-JST channel estimation is derived from (9). We call $\tilde{\mathbf{T}}(\boldsymbol{\theta},\boldsymbol{\gamma},\boldsymbol{\tau})$ the matrix in (9), which is known as a priori from the DT, but limited to $\tilde{P}$ paths. Let $\tilde{\mathbf{U}}_\mathrm{ST} \in \mathbb{C}^{N_\mathrm{R}N_\mathrm{T}W\times\tilde{r}_\mathrm{ST}}$ be the corresponding orthonormal basis (ST propagation modes), such that $\mathrm{span}(\tilde{\mathbf{T}}(\boldsymbol{\theta},\boldsymbol{\gamma},\boldsymbol{\tau})) \equiv \mathrm{span}(\tilde{\mathbf{U}}_\mathrm{ST})$. Also, let $\tilde{r}_\mathrm{ST} = \mathrm{rank}(\tilde{\mathbf{T}}(\boldsymbol{\theta},\boldsymbol{\gamma},\boldsymbol{\tau}))$ be the dimension of the ST subspace obtained from the DT. We remark that, the DT allows us to pre-compute and maintain during the channel's ST invariance period the a priori basis, by exploiting the knowledge on a limited subset of AoAs, AoDs, and delays. These bases $\{\tilde{\mathbf{U}}_\mathrm{ST}\}$ are obtained, as a priori, from the singular value decomposition of $\{\tilde{\mathbf{T}}(\boldsymbol{\theta},\boldsymbol{\gamma},\boldsymbol{\tau})\}$, with computational complexity $O(N_\mathrm{R}N_\mathrm{T}W\tilde{P}^2)$. It follows that, the projection matrix, related to the ST propagation modes is

$$\tilde{\boldsymbol{\Pi}}_\mathrm{ST} = \tilde{\mathbf{U}}_\mathrm{ST}\tilde{\mathbf{U}}_\mathrm{ST}^\mathsf{H}. \tag{10}$$

Afterwards, the DT-JST channel estimates become

$$\hat{\boldsymbol{h}}_m^\mathrm{JST} = \tilde{\boldsymbol{\Pi}}_\mathrm{ST}\hat{\boldsymbol{h}}_m^\mathrm{LS}, \tag{11}$$

where $\hat{\boldsymbol{h}}_m^\mathrm{LS}$ is the LS, or equivalently the maximum-likelihood (ML), channel estimate [12].

### B. DT-S and DT-T method

Differently from the DT-JST, the DT-S and DT-T follow from (6). Similarly, we call $\tilde{\mathbf{S}}(\boldsymbol{\theta},\boldsymbol{\gamma})$ and $\tilde{\mathbf{G}}(\boldsymbol{\tau})$ the matrices in (6), which are known as a priori from the DT, and still limited to $\tilde{P}$ paths. Let $\tilde{\mathbf{U}}_\mathrm{S} \in \mathbb{C}^{N_\mathrm{R}N_\mathrm{T}\times\tilde{r}_\mathrm{S}}$ and $\tilde{\mathbf{U}}_\mathrm{T} \in \mathbb{C}^{W\times\tilde{r}_\mathrm{T}}$ be the corresponding orthonormal basis (space and time propagation modes), such that $\mathrm{span}(\tilde{\mathbf{S}}(\boldsymbol{\theta},\boldsymbol{\gamma})) \equiv \mathrm{span}(\tilde{\mathbf{U}}_\mathrm{S})$ and $\mathrm{span}(\tilde{\mathbf{G}}(\boldsymbol{\tau})) \equiv \mathrm{span}(\tilde{\mathbf{U}}_\mathrm{T})$. Also, let $\tilde{r}_\mathrm{S} = \mathrm{rank}(\tilde{\mathbf{S}}(\boldsymbol{\theta},\boldsymbol{\gamma}))$ and $\tilde{r}_\mathrm{T} = \mathrm{rank}(\tilde{\mathbf{G}}(\boldsymbol{\tau}))$ be the dimensions of the spatial and temporal subspace obtained from the DT, respectively. These bases $\{\tilde{\mathbf{U}}_\mathrm{S},\tilde{\mathbf{U}}_\mathrm{T}\}$ are obtained, as a priori, from the singular

value decomposition of $\{\tilde{\mathbf{S}}(\boldsymbol{\theta},\boldsymbol{\gamma}), \tilde{\mathbf{G}}(\boldsymbol{\tau})\}$, with computational complexity $O(N_{\mathrm{R}}N_{\mathrm{T}}\tilde{P}^2)$ and $O(W\tilde{P}^2)$, respectively. The projection matrices, related to the space and time propagation modes are

$$\tilde{\boldsymbol{\Pi}}_{\mathrm{S}} = \tilde{\mathbf{U}}_{\mathrm{S}}\tilde{\mathbf{U}}_{\mathrm{S}}^{\mathsf{H}}, \quad \tilde{\boldsymbol{\Pi}}_{\mathrm{T}} = \tilde{\mathbf{U}}_{\mathrm{T}}\tilde{\mathbf{U}}_{\mathrm{T}}^{\mathsf{H}}. \tag{12}$$

Accordingly, the DT-S and DT-T channel estimates become, respectively [11]

$$\hat{\boldsymbol{h}}_m^{\mathrm{S}} = \big(\mathbf{I}_W \otimes \tilde{\boldsymbol{\Pi}}_{\mathrm{S}}\big)\hat{\boldsymbol{h}}_m^{\mathrm{LS}}, \quad \hat{\boldsymbol{h}}_m^{\mathrm{T}} = \big(\tilde{\boldsymbol{\Pi}}_{\mathrm{T}}^{*} \otimes \mathbf{I}_{N_{\mathrm{T}}N_{\mathrm{R}}}\big)\hat{\boldsymbol{h}}_m^{\mathrm{LS}}, \tag{13}$$

where $\tilde{\boldsymbol{\Pi}}_{\mathrm{DT-S}} = \mathbf{I}_W \otimes \tilde{\boldsymbol{\Pi}}_{\mathrm{S}}$ and $\tilde{\boldsymbol{\Pi}}_{\mathrm{DT-T}} = \tilde{\boldsymbol{\Pi}}_{\mathrm{T}}^{*} \otimes \mathbf{I}_{N_{\mathrm{T}}N_{\mathrm{R}}}$ denote the projection matrices for the DT-S and DT-T LR channel estimation methods, respectively.

### C. NMSE Analysis

In order to derive the NMSE across pilot subcarriers for the proposed methods, we assume perfect accuracy of the AoAs, AoDs, and delays, as the inherent errors in the 3D model of the environment and ray-tracing simulations are beyond the scope of this paper. Accordingly, the NMSE for the DT-JST estimator $\hat{\boldsymbol{h}}_m^{\mathrm{JST}}$ results in

$$\begin{aligned}\mathrm{NMSE}_{\mathrm{JST}} &= \frac{\mathrm{Tr}\big\{\mathbb{E}\{\|\boldsymbol{h}_m - \hat{\boldsymbol{h}}_m^{\mathrm{JST}}\|^2\}\big\}}{\mathrm{Tr}\big\{\mathbb{E}\{\|\boldsymbol{h}_m\|^2\}\big\}} \\ &= \frac{\mathrm{Tr}\big\{\tilde{\boldsymbol{\Pi}}_{\mathrm{ST}}^{\perp}\mathbf{R}_{\boldsymbol{h}}\big\}}{\mathrm{Tr}\big\{\mathbf{R}_{\boldsymbol{h}}\big\}} + \frac{\tilde{r}_{\mathrm{ST}}}{WN_{\mathrm{T}}N_{\mathrm{R}}(\frac{N_{\mathrm{P}}}{N_{\mathrm{sc}}})\mathrm{SNR}} \\ &= \sigma^2_{\tilde{P},\mathrm{JST}} + \sigma^2_{\tilde{w},\mathrm{JST}},\end{aligned} \tag{14}$$

where $\mathbf{R}_{\boldsymbol{h}}$ denotes the covariance matrix of the ST MIMO channel, $\tilde{\boldsymbol{\Pi}}_{\mathrm{ST}}^{\perp} = (\mathbf{I}_{WN_{\mathrm{T}}N_{\mathrm{R}}} - \tilde{\boldsymbol{\Pi}}_{\mathrm{ST}})$ represents the orthonormal projection matrix to $\tilde{\boldsymbol{\Pi}}_{\mathrm{ST}}$, and $\mathrm{SNR} = \frac{\eta\beta}{\sigma_w^2}$, with $\beta = \frac{\mathrm{Tr}\{\mathbf{R}_{\boldsymbol{h}}\}}{WN_{\mathrm{T}}N_{\mathrm{R}}}$ being the average channel gain. In (14), the term $\sigma^2_{\tilde{P},\mathrm{JST}}$ accounts for the projection error power due to the limited number of paths. Notably, this term must satisfy

$$0 \le \sigma^2_{\tilde{P},\mathrm{JST}} \le 1. \tag{15}$$

Specifically, $\sigma^2_{\tilde{P},\mathrm{JST}} = 0$ occurs in case of complete characterization of the multi-path propagation environment, hence when $\boldsymbol{\Pi}_{\mathrm{ST}} = \tilde{\boldsymbol{\Pi}}_{\mathrm{ST}}$, and follows that, $\mathrm{Tr}\{\tilde{\boldsymbol{\Pi}}_{\mathrm{ST}}^{\perp}\mathbf{R}_{\boldsymbol{h}}\} = \mathrm{Tr}\{\mathbf{R}_{\boldsymbol{h}} - \boldsymbol{\Pi}_{\mathrm{ST}}\mathbf{R}_{\boldsymbol{h}}\} = 0$. Conversely, $\sigma^2_{\tilde{P},\mathrm{JST}} = 1$ results from the complete lack of prior information. In this case, $\tilde{\boldsymbol{\Pi}}_{\mathrm{ST}}^{\perp} = \mathbf{I}_{WN_{\mathrm{R}}N_{\mathrm{T}}}$, and as a consequence $\mathrm{Tr}\{\tilde{\boldsymbol{\Pi}}_{\mathrm{ST}}^{\perp}\mathbf{R}_{\boldsymbol{h}}\} = \mathrm{Tr}\{\mathbf{R}_{\boldsymbol{h}}\}$. On the other hand, the term $\sigma^2_{\tilde{w},\mathrm{JST}}$ accounts for the projected noise power onto the subspace spanned by the columns of $\tilde{\mathbf{U}}_{\mathrm{ST}}$. It is straightforward to show that

$$0 \le \sigma^2_{\tilde{w},\mathrm{JST}} \le \frac{r_{\mathrm{ST}}}{WN_{\mathrm{T}}N_{\mathrm{R}}(\frac{N_{\mathrm{P}}}{N_{\mathrm{sc}}})\mathrm{SNR}}. \tag{16}$$

Precisely, $\sigma^2_{\tilde{w},\mathrm{JST}} = \frac{r_{\mathrm{ST}}}{WN_{\mathrm{T}}N_{\mathrm{R}}(\frac{N_{\mathrm{P}}}{N_{\mathrm{sc}}})\mathrm{SNR}}$ corresponds to a complete characterization of the propagation environment, while $\sigma^2_{\tilde{w},\mathrm{JST}} = 0$ is achieved when no prior information is available.

The above observation are similarly extended to the DT-S and DT-T methods. However, it is important to note that the projection matrices differ from that of the DT-JST method. Accordingly, the projection error due to the limited number of paths, and the term accounting for the projection of noise, for the DT-S and DT-T are illustrated in Table I, where a comparison of $\sigma^2_{\tilde{P}}$ and $\sigma^2_{\tilde{w}}$ is shown for our proposed approaches, the DT-SST [7], and the conventional LS. Note that the projection matrix for the DT-SST [7] is $\tilde{\boldsymbol{\Pi}}_{\mathrm{SST}} = \tilde{\boldsymbol{\Pi}}_{\mathrm{T}}^{*} \otimes \tilde{\boldsymbol{\Pi}}_{\mathrm{S}}$.

| **Method** | $\sigma^2_{\tilde{P}}$ | $\sigma^2_{\tilde{w}}$ |
|---|---|---|
| DT − JST | $\frac{\mathrm{Tr}\{\tilde{\boldsymbol{\Pi}}_{\mathrm{ST}}^{\perp}\mathbf{R}_{\boldsymbol{h}}\}}{\mathrm{Tr}\{\mathbf{R}_{\boldsymbol{h}}\}}$ | $\frac{\tilde{r}_{\mathrm{ST}}}{WN_{\mathrm{T}}N_{\mathrm{R}}(\frac{N_{\mathrm{P}}}{N_{\mathrm{sc}}})\mathrm{SNR}}$ |
| DT − SST [7] | $\frac{\mathrm{Tr}\{\tilde{\boldsymbol{\Pi}}_{\mathrm{SST}}^{\perp}\mathbf{R}_{\boldsymbol{h}}\}}{\mathrm{Tr}\{\mathbf{R}_{\boldsymbol{h}}\}}$ | $\frac{\tilde{r}_{\mathrm{S}}\tilde{r}_{\mathrm{T}}}{WN_{\mathrm{T}}N_{\mathrm{R}}(\frac{N_{\mathrm{P}}}{N_{\mathrm{sc}}})\mathrm{SNR}}$ |
| DT − S | $\frac{\mathrm{Tr}\{\tilde{\boldsymbol{\Pi}}_{\mathrm{DT-S}}^{\perp}\mathbf{R}_{\boldsymbol{h}}\}}{\mathrm{Tr}\{\mathbf{R}_{\boldsymbol{h}}\}}$ | $\frac{\tilde{r}_{\mathrm{S}}}{N_{\mathrm{T}}N_{\mathrm{R}}(\frac{N_{\mathrm{P}}}{N_{\mathrm{sc}}})\mathrm{SNR}}$ |
| DT − T | $\frac{\mathrm{Tr}\{\tilde{\boldsymbol{\Pi}}_{\mathrm{DT-T}}^{\perp}\mathbf{R}_{\boldsymbol{h}}\}}{\mathrm{Tr}\{\mathbf{R}_{\boldsymbol{h}}\}}$ | $\frac{\tilde{r}_{\mathrm{T}}}{W(\frac{N_{\mathrm{P}}}{N_{\mathrm{sc}}})\mathrm{SNR}}$ |
| LS | 0 | $\frac{1}{(\frac{N_{\mathrm{P}}}{N_{\mathrm{sc}}})\mathrm{SNR}}$ |

TABLE I: Projection error power $\sigma^2_{\tilde{P}}$ and projected noise power $\sigma^2_{\tilde{w}}$ for our investigated approaches, for the DT-SST [7], and for the conventional LS.

## IV. Numerical results

Consistently with the system model in Sec. II, we set $N = 128$, $N_{\mathrm{R}} = 64$, and $N_{\mathrm{T}} = 4$. We allocate $N_{\mathrm{p}} = 64$ pilots on each training OFDM symbol and we consider numerology $\mu = 4$ of 5G NR frame, corresponding to a subcarrier spacing of $\Delta f = 240$KHz and to an overall bandwidth $B = 30.72$MHz. The simulated benchmark channel is generated by means of a commercial ray-tracer with $P = 25$ paths with a carrier frequency $f_c = 28$ GHz. Additionally, the temporal support length of the channel is $W = 10$ OFDM samples, and corresponds to the CP length $N_{cp}$.

Figures 2a and 2b illustrate the NMSE comparison for different methods, considering $\tilde{P} = 1$ and $\tilde{P} = 7$ available number of paths provided by the DT, respectively. For $\tilde{P} = 1$, the DT-JST and DT-SST methods outperform the DT-S, DT-T, and LS, the low SNR region. However, due to the partial lack of multipath propagation components, these methods reach a threshold, posed by $\sigma^2_{\tilde{P}}$, at approximately $\mathrm{SNR} = -10$ dB. In contrast, the DT-T approach maintains superior performance over LS, even in the high SNR region, proving its robustness to the limited prior information. When $\tilde{P} = 7$, all DT-empowered methods exhibit saturation at higher SNR values. Within the SNR values of interest, the DT-JST and DT-SST approaches achieve higher performance than DT-S, DT-T, and LS. Specifically, the DT-JST provides an approximate gain of 25 dB over LS, while DT-SST achieves a gain of about 20 dB. Accordingly, when rich prior information on the multipath components of the propagation environment is available, these methods are desirable in comparison to the DT-S, DT-T, and LS approaches.

Figure 3 illustrates the comparison between the projection error power $\sigma^2_{\tilde{P}}$, for the proposed approaches, against the

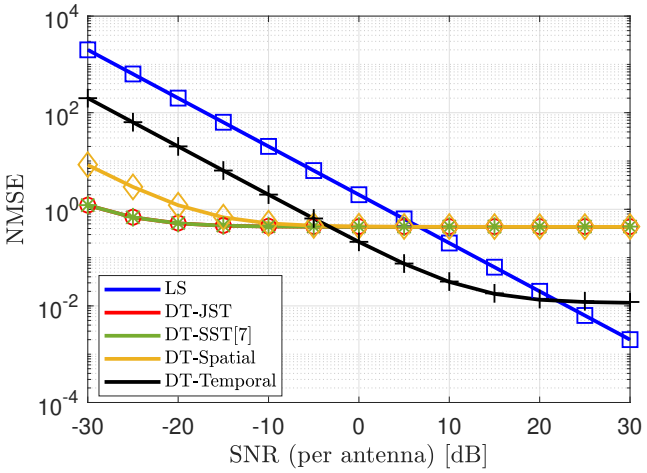


(a)

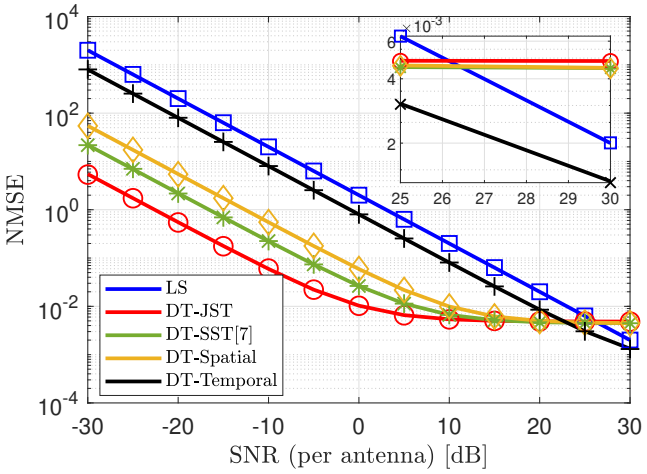


(b)

Fig. 2: NMSE Comparison for a) $\tilde{P} = 1$ path and b) $\tilde{P} = 7$ paths, for the proposed approaches, the DT-SST [7], and for the conventional LS. Solid lines denote the analytical NMSE, while markers are the simulated results.

NMSE for the LS, at SNR $= 20$ dB and SNR $= 30$ dB. As observed, among the investigated methods, the DT-T approach demonstrates greater robustness to limited prior knowledge, whereas the DT-JST is the most sensitive. Specifically, the DT-T achieves a projection error power $\sigma^2_{\tilde{P}}$ lower than the NMSE of the LS estimator at SNR $= 20$ dB with only a single path, whereas at least three paths are required for the same condition at SNR $= 30$ dB. In contrast, the DT-JST, DT-SST, and DT-S necessitate at least 3 paths to ensure that $\sigma^2_{\tilde{P}}$ remains below the NMSE of the LS at SNR $= 20$ dB, while more than 12 paths are needed at SNR $= 30$ dB. Based on these results, we conclude that only a few paths are needed to approximate the ground-truth temporal subspace, while a larger number of multipath components are required to capture the ground-truth spatial subspace.

Finally, as observed in Figures 4a and 4b, limited prior

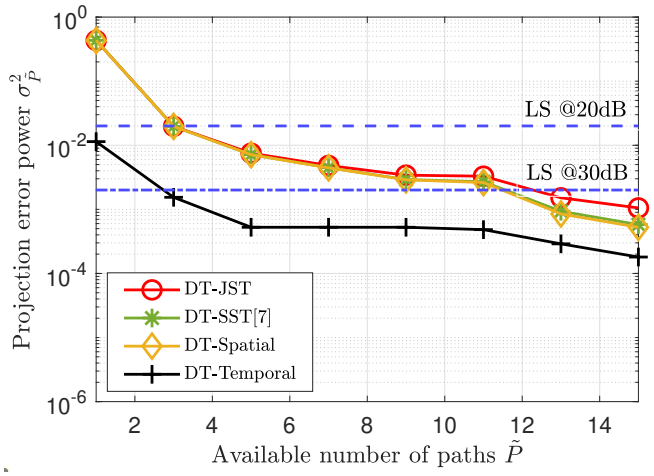


Fig. 3: Comparison of the analytical values of the projection error power $\sigma^2_{\tilde{P}}$, for the proposed approaches and DT-SST [7], against the NMSE for LS at SNR $= 20$ dB and SNR $= 30$ dB.

knowledge enables modal projection of noise onto a restricted subspace in comparison to the ground-truth. Specifically, as the number of known paths increases, the projected noise power $\sigma^2_{\tilde{w}}$ also increases. Moreover, for the DT-T method at SNR $= 10$ dB, $\sigma^2_{\tilde{w}} > \sigma^2_{\tilde{P}}$, meaning that the NMSE is primarily affected by $\sigma^2_{\tilde{w}}$. Conversely, for the remaining DT-empowered channel estimation methods, this inequality does not hold when only few paths are considered. As a result, the NMSE is constrained by the threshold set by $\sigma^2_{\tilde{P}}$, when few paths are provided by the DT. A similar behaviour is observed for SNR $= 20$ dB. However, in this case, all methods exhibit a certain number of paths at which $\sigma^2_{\tilde{w}} < \sigma^2_{\tilde{P}}$ and hence, the NMSE reaches the threshold imposed by $\sigma^2_{\tilde{P}}$, confirming the results of Figures 2a and 2b.

## V. Conclusion

This paper proposes three distinct DT-empowered LR methods for channel estimation; a DT-JST, DT-S, and DT-T. These methods leverage a priori information on AoAs, AoDs, and delays, provided by the DT. Each approach performs modal projection onto a different subspace, namely, joint spatial-temporal, spatial, and temporal subspace. Furthermore, we provide, for the first time, a theoretical analysis of the NMSE and compare our methods against the DT-SST [7] and the conventional LS approach, under limited number of paths provided by DT. Simulation results demonstrate that, under limited prior information, the DT-T method achieves superior performance in the high SNR region, in terms of NMSE, compared to DT-JST, DT-S, and DT-SST [7]. Conversely, when accurate prior information is available, DT-JST outperforms all other methods. Specifically, the DT-T method provides a gain of approximately 5 dB over LS when only a single path is provided, for an SNR range of $-30$ dB to approximately 15 dB. Meanwhile, DT-JST achieves a gain of roughly 25 dB over LS for an SNR ranging from $-30$ dB to 10 dB, when

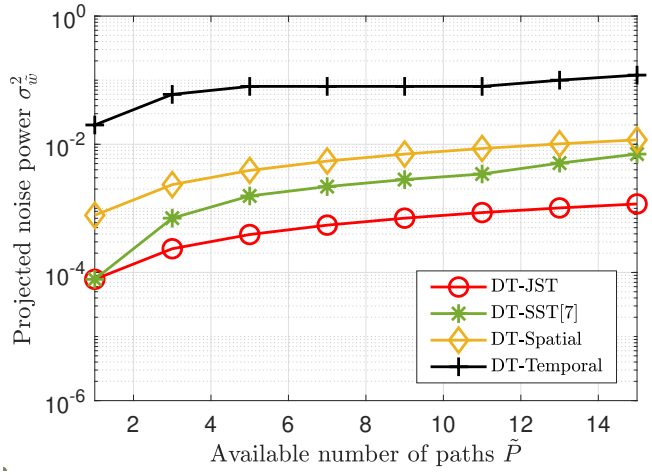


(a)

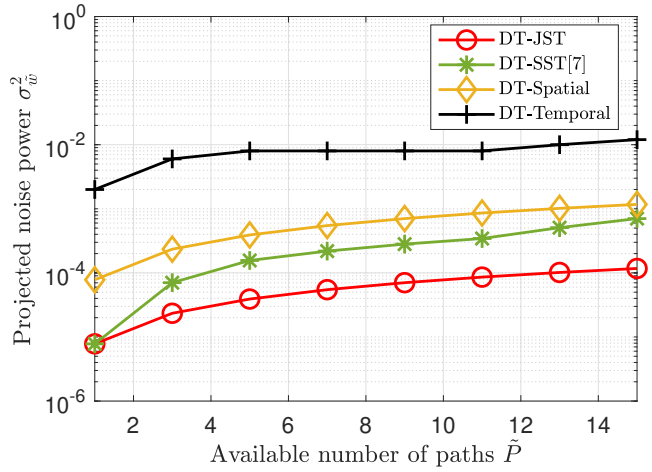


(b)

Fig. 4: Comparison of the analytical values of the projected noise power $\sigma^2_{\tilde{w}}$ for a) SNR $= 10$ dB and b) SNR $= 20$ dB, for the proposed approaches and DT-SST [7].

7 paths are known from the DT. According to these results, when few paths are provided by DT, modal projection must be performed only onto the temporal subspace, in order to limit the projection error due to the lack of multipath components. Conversely, when rich prior information is present, projection on both subspaces is desirable. Additionally, further investigation is required to analyze the impact of errors in the 3D model of the environment or in the UE's estimated position.

## REFERENCES

[1] E. G. Larsson, O. Edfors, F. Tufvesson, and T. L. Marzetta, "Massive mimo for next generation wireless systems," *IEEE Communications Magazine*, vol. 52, no. 2, pp. 186–195, 2014.

[2] T. S. Rappaport, S. Sun, R. Mayzus, H. Zhao, Y. Azar, K. Wang, G. N. Wong, J. K. Schulz, M. Samimi, and F. Gutierrez, "Millimeter wave mobile communications for 5g cellular: It will work!" *IEEE Access*, vol. 1, pp. 335–349, 2013.

[3] C.-X. Wang, X. You, X. Gao, X. Zhu, Z. Li, C. Zhang, H. Wang, Y. Huang, Y. Chen, H. Haas, J. S. Thompson, E. G. Larsson, M. D. Renzo, W. Tong, P. Zhu, X. Shen, H. V. Poor, and L. Hanzo, "On the road to 6g: Visions, requirements, key technologies, and testbeds," *IEEE Communications Surveys & Tutorials*, vol. 25, no. 2, pp. 905–974, 2023.

[4] A. Alkhateeb, S. Jiang, and G. Charan, "Real-time digital twins: Vision and research directions for 6g and beyond," *IEEE Communications Magazine*, vol. 61, no. 11, pp. 128–134, 2023.

[5] M. Zhu, L. Cazzella, F. Linsalata, M. Magarini, M. Matteucci, and U. Spagnolini, "Toward real-time digital twins of EM environments: Computational benchmark for ray launching software," *IEEE Open Journal of the Communications Society*, 2024.

[6] R. Pegurri, F. Linsalata, E. Moro, J. Hoydis, and U. Spagnolini, "Toward digital network twins: Integrating sionna RT in ns-3 for 6G Multi-RAT networks simulations," in *IEEE INFOCOM WKSHPS: Digital Twins over NextG Wireless Networks (DTWIN 2025) (INFOCOM DTWIN 2025)*, London, United Kingdom (Great Britain), May 2025, p. 6.

[7] L. D. Moro, F. Linsalata, M. Mizmizi, M. Magarini, D. Badini, and U. Spagnolini, "Bayesian em digital twins channel estimation," *IEEE Wireless Communications Letters*, pp. 1–1, 2025.

[8] S. Alikhani and A. Alkhateeb, "Digital twin aided channel estimation: Zone-specific subspace prediction and calibration," 2025. [Online]. Available: https://arxiv.org/abs/2501.02758

[9] M. Cicerone, O. Simeone, and U. Spagnolini, "Channel estimation for mimo-ofdm systems by modal analysis/filtering," *IEEE Transactions on Communications*, vol. 54, no. 11, pp. 2062–2074, 2006.

[10] C. Ruah, O. Simeone, J. Hoydis, and B. Al-Hashimi, "Calibrating wireless ray tracing for digital twinning using local phase error estimates," *IEEE Transactions on Machine Learning in Communications and Networking*, vol. 2, pp. 1193–1215, 2024.

[11] A. Brighente, M. Cerutti, M. Nicoli, S. Tomasin, and U. Spagnolini, "Estimation of wideband dynamic mmwave and thz channels for 5g systems and beyond," *IEEE Journal on Selected Areas in Communications*, vol. 38, no. 9, pp. 2026–2040, 2020.

[12] I. Barhumi, G. Leus, and M. Moonen, "Optimal training design for mimo ofdm systems in mobile wireless channels," *IEEE Transactions on Signal Processing*, vol. 51, no. 6, pp. 1615–1624, 2003.

[13] E. Björnson and Demir, *Introduction to Multiple Antenna Communications and Reconfigurable Surfaces*, 01 2024.

[14] M. Mizmizi, D. Tagliaferri, D. Badini, C. Mazzucco, and U. Spagnolini, "Channel estimation for 6g v2x hybrid systems using multi-vehicular learning," *IEEE Access*, vol. 9, pp. 95 775–95 790, 2021.